The Meteoritical Society

Meteoritics & Planetary Science 47, Nr 9, 1419–1435 (2012)
doi: 10.1111/j.1945-5100.2012.01404.x

Petrogenesis of Grove Mountains 020090: An enriched "lherzolitic" shergottite

Yun JIANG[1] and Weibiao HSU[2*]

[1]Laboratory for Astrochemistry and Planetary Sciences, Purple Mountain Observatory, Chinese Academy of Sciences, Nanjing 210008, China
[2]State Key Laboratory of Geological Processes and Mineral Resources, Faculty of Earth Sciences, China University of Geosciences, Wuhan 430074, China
[*]Corresponding author. E-mail: wbxu@pmo.ac.cn

(Received 19 January 2012; revision accepted 15 July 2012)

Abstract–Grove Mountains (GRV) 020090 is a "lherzolitic" shergottite found in the Grove Mountains, Antarctica. It exhibits two distinct textures: poikilitic and nonpoikilitic. In poikilitic areas, large pyroxene oikocrysts enclose subhedral olivine and chromite chadacrysts. Pyroxene oikocrysts are zoned from pigeonite cores to augite rims. In nonpoikilitic areas, olivine, pyroxene, and interstitial maskelynite occur as major phases, and minor phases include chromite and merrillite. Compared with typical "lherzolitic" shergottites, GRV 020090 contains a distinctly higher abundance of maskelynite (19 vol%). Olivine and pyroxene are more ferroan ($Fa_{28–40}$, $En_{57–72}Fs_{24–31}Wo_{4–14}$ and $En_{46–53}Fs_{17–21}Wo_{26–35}$), and maskelynite is more alkali-rich ($Ab_{43–65}Or_{2–7}$). The major phases, whole-rock (estimated) and fusion crust of GRV 020090, are relatively enriched in light rare earth elements (LREE), similar to those of the geochemically enriched basaltic shergottites, but distinct from those of LREE-depleted "lherzolitic" shergottites. Combined with a high oxygen fugacity of log fO_2 = QFM − 1.41 ± 0.04 (relative to the quartz-fayalite-magnetite buffer), it is clear that GRV 020090 sampled from an oxidized and enriched mantle reservoir similar to those of other enriched shergottites. The calculated REE abundances and patterns of the melts in equilibrium with the cores of major phases are parallel to but higher than that of the whole rock, suggesting that GRV 020090 originated from a single parent magma and experienced progressive fractional crystallization in a closed system. The crystallization age recorded by baddeleyite is 192 ± 10 (2σ) Ma, consistent with the young internal isochron ages of enriched shergottites. Baddeleyite dating results further demonstrated that the young ages, rather than ancient ages (>4 Ga), appear to represent the crystallization of Martian surface lava flow. GRV 020090 shares many similarities with Roberts Massif (RBT) 04261/2, the first enriched "lherzolitic" shergottite. Detailed comparisons suggest that these two rocks are petrologically and geochemically closely related, and probably launch paired.

INTRODUCTION

Shergottite, nakhlite, chassignite, and Allan Hills (ALH) 84001 meteorites are believed to have originated from Mars. As the main group of Martian meteorites (50 of 61 samples), shergottites exhibit a variety of mineralogies. Petrologically, shergottites are divided into three subgroups: basaltic, olivine-phyric, and lherzolitic (Goodrich 2002). Basaltic shergottites mainly consist of pyroxene (pigeonite and augite) and plagioclase. Olivine-phyric shergottites consist of olivine megacrysts and groundmass of pyroxene and plagioclase. Lherzolitic shergottites are olivine–pyroxene cumulates. They usually have two types of lithologies: a poikilitic region consisting of pyroxene oikocrysts enclosing subhedral olivine and chromite inclusions, and a nonpoikilitic one consisting of olivine, pigeonite, augite with interstitial maskelynite. Based on trace element abundances and radiogenic isotopic compositions, shergottites can also be classified into three geochemical subgroups: depleted, enriched, and intermediate (Symes et al. 2008). Depleted shergottites sampled a reduced, light rare earth elements

(LREE)-depleted reservoir with low initial Sr and high initial Nd isotopic compositions (e.g., QUE 94201, DaG 476), whereas enriched shergottites sampled an oxidized, LREE-enriched reservoir with high initial Sr and low initial Nd isotopic compositions (e.g., Shergotty, LAR 06319) (Wadhwa 2001; Borg et al. 2002; Herd et al. 2002). Both basaltic and olivine-phyric shergottites have depleted, enriched, and intermediate samples (Wadhwa et al. 1994; Symes et al. 2008). In contrast, lherzolitic shergottites only show an intermediate signature (Borg et al. 2002). Recently, Usui et al. (2010) reported the first enriched lherzolitic shergottite Roberts Massif (RBT) 04261 (and paired RBT 04262), which is petrographically similar to lherzolitic shergottites, but geochemically kin to enriched basaltic shergottites (Anand et al. 2008; Lapen et al. 2008).

Grove Mountains (GRV) 020090 was collected from the ice field of the Grove Mountains, Antarctica, by the 19th Chinese Antarctic Research Expedition in 2002/2003. It was classified as the sixth lherzolitic shergottite after Allan Hills (ALH) A77005, Yamato (Y-) 793605, Lewis Cliff (LEW) 88516, GRV 99027, and Northwest Africa (NWA) 1950 (Miao et al. 2004; Lin et al. 2008a). Lherzolite is defined as a terrestrial ultramafic plutonic rock with 40–90% olivine, > 5% orthopyroxene, and > 5% clinopyroxene (Le Maitre et al. 1989). The low abundance of olivine and the absence of orthopyroxene in existing lherzolitic shergottites make the term "lherzolitic" inappropriate. Mikouchi (2009) suggested a new name "pyroxene-oikocrystic" because of textural characteristics of large pyroxene oikocrysts enclosing olivine. Irving et al. (2010) proposed a classification scheme based on bulk chemical compositions. Due to the conventional usage in the previous literatures, we adhere to "lherzolitic," even though GRV 020090 and RBT 04261/2 are not strictly ultramafic in bulk compositions.

In this paper, we report detailed mineralogy, petrology, trace element chemistry, and U-Pb chronology of baddeleyite in GRV 020090 with the goals to better understand its petrogenesis and related basaltic magma evolution on Mars. Our results show that GRV 020090 is a new geochemically enriched "lherzolitic" shergottite. Direct comparisons of mineralogy, petrology, trace element abundances, and radiometric ages between GRV 020090 and RBT 04261/2 will help understand the petrogenesis of the newly found geochemically enriched "lherzolitic" shergottites.

SAMPLE AND ANALYTICAL TECHNIQUE

GRV 020090 weighs 7.54 g and is completely covered by a fresh fusion crust. The sample used in this study is a one-inch round polished thick section (GRV 020090-1), provided by Polar Research Institute of China. Petrographic observation was made using a Hitachi 3400N II scanning electron microscope (SEM) equipped with an energy-dispersive X-ray spectrometry (EDS). Quantitative mineral chemical analyses were performed using the JEOL 8100 electron microprobe (EMP) at China University of Geosciences, Wuhan. The operating conditions are 15 kV accelerating voltage and 20 nA beam current (10 nA for plagioclase). Typical detection limits for most elements are approximately 0.03 wt%. Natural and synthetic standards were used for calibration, and all data were reduced by the ZAF procedure. Modal abundances were calculated from the back scattered electron (BSE) image. Chromite compositions were calculated using a Microsoft Excel™ worksheet (http://www.open.ac.uk/earth-research/tindle/AGTWebPages/AGTSoft.html).

In situ REE analyses were conducted with an LA-ICP-MS at the State Key Laboratory of Geological Processes and Mineral Resources, China University of Geosciences, Wuhan. Detailed operating conditions for the laser and the ICP-MS instrument were given by Liu et al. (2008). Laser sampling with a spot size of 60 μm was applied using a GeoLas 2005. An Agilent 7500a ICP-MS instrument was used to acquire ion-signal intensities. Helium was applied as a carrier gas. Argon was used as the make-up gas and mixed with the carrier gas via a T-connector before entering the ICP. Each analysis incorporated a background acquisition of approximately 20–30 s (gas blank) followed by 50 s data acquisition from the sample. An Agilent Chemstation was utilized for the acquisition of each analysis. Element contents were calibrated against the USGS reference glasses (BCR-2G, BIR-1G, and BHVO-2G), using silicon and calcium as internal standards for silicates and phosphates, respectively. Every five sample analyses were followed by one analysis of NIST SRM 610 to correct the time-dependent drift of sensitivity and mass discrimination for the trace element analysis. The detection limits are at ppb level. Off-line selection and integration of background and analyte signals, and time-drift correction, and quantitative calibration were performed using the in-house software *ICPMSDataCal* (Liu et al. 2008).

In situ U-Th-Pb isotopic analyses for baddeleyite in GRV 020090 were carried out using the Cameca IMS-1280 secondary ion mass spectrometer (SIMS) at the Institute of Geology and Geophysics of the Chinese Academy of Sciences, following the procedure of Liu et al. (2011). The mono-collector mode was used. The O_2^- primary ion beam was accelerated at −13 kV, with an intensity of approximately 100 pA. A Gaussian illumination mode was used to obtain a small beam size (< 5 μm). Positive secondary ions were extracted with a 10 kV potential. Oxygen flooding (approximately 1.5×10^{-6} Torr in the sample chamber) was introduced to enhance Pb^+ sensitivity (Li et al. 2010). Lead/uranium

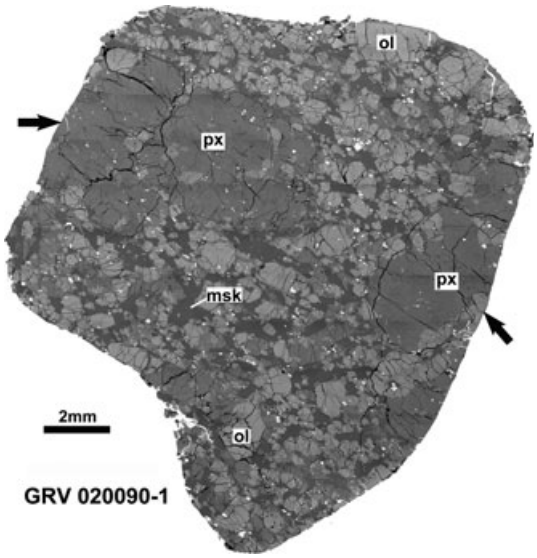

Fig. 1. The back-scattered electron (BSE) image of GRV 020090-1 thick section used in this study. Black arrows indicate the poikilitic areas composed of large pyroxene oikocrysts enclosing olivine and chromite. The nonpoikilitic area mainly consists of olivine, pyroxene, and interstitial maskelynite. px = pyroxene; ol = olivine; msk = maskelynite.

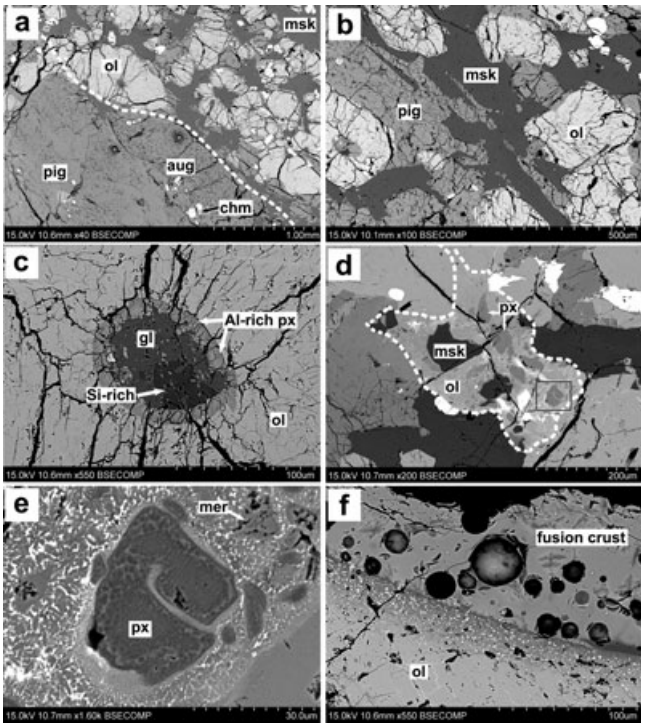

Fig. 2. BSE images of GRV 020090. a) The white dotted line shows the boundary between the poikilitic area (the lower left) and the nonpoikilitic area (the upper right). b) Maskelynite intergrows with pyroxene indicating cocrystallization. c) A magmatic inclusion within an olivine grain is surrounded with radial fractures. It mainly consists of feldspathic glasses and Al-rich pyroxene. The darker part is Si-rich glasses. d) An irregularly shaped melt pocket occurs adjacent to olivine, pyroxene, maskelynite, and chromite in the host rock. e) The enlarged portion shown in (d). Pyroxene shows a recrystallized texture. f) Olivine grain close to the fusion crust is reduced to more Mg-rich olivine (darker) and tiny Fe-metal grains. pig = pigeonite; aug = augite; ol = olivine; chm = chromite; msk = maskelynite; gl = glass; px = pyroxene; mer = merrillite.

ratios were calibrated with a power law relationship between Pb^+/U^+ and UO_2^+/U^+ relative to Phalaborwa baddeleyite standard (2059.6 Ma) (Heaman 2009). Due to the high and variable proportions of common Pb, the total $^{238}U/^{206}Pb$ and $^{207}Pb/^{206}Pb$ data were plotted on a Tera-Wasserburg inverse concordia diagram to deduce the crystallization age and common lead composition (Ludwig 2001). The authors assumed that baddeleyites are cogenetic and they have had no later lead loss. Then a ^{207}Pb-correction method was applied to single analytical point (Li et al. 2012).

RESULTS

Petrography

The GRV 020090-1 section is 1.7×1.5 cm^2 in size with an area of 2.1 cm^2. It exhibits two distinct textures: poikilitic and nonpoikilitic (Fig. 1). The poikilitic area (30%) is smaller than the nonpoikilitic area (70%). The boundary between the two parts is relatively clear (Fig. 2a). In poikilitic areas, large pyroxene oikocrysts (up to 8.6 mm) enclose subhedral olivine and chromite chadacrysts. Pyroxene oikocrysts are zoned from low-Ca pyroxene cores to high-Ca pyroxene rims. Olivine chadacrysts range from 150 to 1300 μm in size with an average of 540 μm. Chromite chadacrysts are usually small (approximately 50 μm). In the nonpoikilitic area, olivine, low-Ca pyroxene, and interstitial maskelynite are major phases, and minor phases include high-Ca pyroxene, chromite, merrillite, sulfide, ilmenite, and rare baddeleyite. The modal abundances of two areas and the whole section are listed in Table 1.

Euhedral olivine grains in the nonpoikilitic area are larger (up to 1.8 mm) than those in the poikilitic area. Most pyroxene and maskelynite are in the size of approximately 500 μm and occasionally show intergrown texture indicating cocrystallization (Fig. 2b). X-ray mapping shows that high-Ca pyroxene occurs as a rim (up to approximately 1 mm thick) surrounding low-Ca pyroxene oikocrysts (Fig. 2a), or as a large individual grain (up to 2 mm) in the nonpoikilitic area. Merrillite and ilmenite are mainly present in the nonpoikilitic area.

Magmatic inclusions and chromite grains are commonly observed within olivine grains in both areas, but rarely in pyroxene and maskelynite. The inclusions are usually ovoid (approximately 100 μm in size), and often surrounded by radial fractures (Fig. 2c). They

Table 1. Modal abundances of the GRV 020090-1 section and other shergottites (vol%).

	Poikilitic (30.6%)	Nonpoikilitic (69.4%)	Bulk (100%)	RBT 04261	RBT 04262	RBT 04262*	ALHA77005	Shergotty
Olivine	10.9	36	28.3	42.1	39.4	30	52	
Low-Ca pyroxene	60.1	29.3	38.7	21.5	28.0	43	26	36.3
High-Ca pyroxene	28.1	4.2	11.5	10.7	12.4	10	11	33.5
Chromite	0.9	1.6	1.4	1.6	1.5	2	1	
Maskelynite	+	27.3	18.9	20.2	15.9	13	10	23.3
Merrillite	+	1.4	1.0	1.8	1.1	1		
Sulfide	+	0.2	0.1	0.3	0.3			
Ilmenite	−	+	+	0.2	0.2			
Titanomagnetite								2.3
Mesostasis intergrowth								4.0

− = not found; + = minor.

"Lherzolitic" shergottites: RBT 04261 and RBT 04262 (Usui et al. 2010; RBT 04262* from Mikouchi et al. 2008), ALHA77005 (Ma et al. 1981); Basaltic shergottite: Shergotty (Stolper and McSween 1979).

Table 2. Representative EMP analyses of minerals in GRV 020090 (wt%).

	Olivine			Pigeonite		Augite			Maskelynite		Chromite		Ilmenite	Merrillite	Baddeleyite
	P	NP		P	NP	P	NP		NP		P	NP	NP	NP	NP
SiO_2	36.48	35.68		54.59	53.98	51.91	51.76		57.71		0.16	0.24	0.13	0.11	0.38
TiO_2	0.05	0.06		0.15	0.31	0.31	0.28		0.08		1.52	12.06	50.99	b.d.	1.53
Al_2O_3	0.08	0.07		0.66	1.05	1.60	1.47		26.00		8.65	4.66	0.10	0.03	0.09
Cr_2O_3	0.07	0.01		0.35	0.39	0.79	0.65		b.d.		50.61	29.85	0.76	b.d.	0.02
FeO	29.96	32.53		16.22	18.06	10.90	11.63		0.50		32.55	48.17	43.08	1.00	1.85
MnO	0.60	0.63		0.61	0.59	0.40	0.39		b.d.		0.54	0.60	0.72	0.06	b.d.
MgO	31.55	29.30		23.40	21.17	16.73	16.72		0.11		4.51	3.22	3.63	3.11	0.05
CaO	0.24	0.20		3.49	4.33	15.88	15.44		9.07		b.d.	b.d.	0.07	47.28	0.05
Na_2O	0.04	b.d.		0.09	0.07	0.25	0.19		5.87		b.d.	0.02	b.d.	1.78	b.d.
K_2O	b.d.	0.02		0.01	b.d.	0.02	b.d.		0.35		b.d.	0.01	b.d.	0.07	b.d.
P_2O_5	n.d.	n.d.		n.d.	n.d.	n.d.	n.d.		n.d.		n.d.	n.d.	n.d.	45.88	n.d.
ZrO_2	n.d.	n.d.		n.d.	n.d.	n.d.	n.d.		n.d.		n.d.	n.d.	n.d.	n.d.	93.25
HfO_2	n.d.	n.d.		n.d.	n.d.	n.d.	n.d.		n.d.		n.d.	n.d.	n.d.	n.d.	2.37
Total	99.06	98.51		99.57	99.94	98.79	98.53		99.69		98.55	98.83	99.47	99.33	99.58
Fa	34.8	38.4	En	66.8	61.5	48.8	48.7	An	45.1	Chm	70	42.6			
			Fs	26.0	29.4	17.9	19.0	Ab	52.9	Sp	18	9.9			
			Wo	7.2	9.0	33.3	32.3	Or	2.1	Mt	8	14.8			
										Usp	4	32.7			

P = poikilitic; NP = onpoikilitic; b.d. = below detection limit; n.d. = not detected.

Chm = 100 × molar Cr/(Cr + 2Ti + Al + Fe^{3+}); Sp = 100 × molar Al/(Cr + 2Ti + Al + Fe^{3+}); Mt = 100 × molar Fe^{3+}/(Cr + 2Ti + Al + Fe^{3+}); Usp = 100 × molar 2Ti/(Cr + 2Ti + Al + Fe^{3+}).

consist predominantly of feldspathic glasses and Al-rich pyroxenes (both low- and high-Ca pyroxenes) which either embed in the glass or occur as rims along the walls of inclusions. Other phases in the inclusions are Si-rich grains (probably SiO_2), merrillite, ilmenite, sulfide, and chromite.

Olivine and pyroxene are heavily fractured. Plagioclase was completely converted into maskelynite due to the shock effect. We also observed one irregularly shaped shock-induced melt pocket (approximately 200 μm in width) in the nonpoikilitic area (Figs. 2d and 2e). Mineral fragments of pyroxene, olivine, maskelynite, chromite, and merrillite are set in the groundmass of glass, micro-crystallites, merrillite, stringers of chromite, and immiscible sulfides. Pyroxene shows a recrystallized texture (Fig. 2e), while chromite exhibits vesiculated internal texture.

Olivine adjacent to the fusion crust shows a texture of iron reduction, consisting of tiny iron metal grains and Mg-rich olivine (Fig. 2f). Pyroxene exhibits a similar texture, too. This feature has also been observed in the "lherzolitic" shergottite NWA 1950 and chassignite NWA 2737 (Mikouchi 2005; Van de Moortèle et al. 2007).

Mineral Chemistry

The representative mineral compositions of GRV 020090 are given in Table 2.

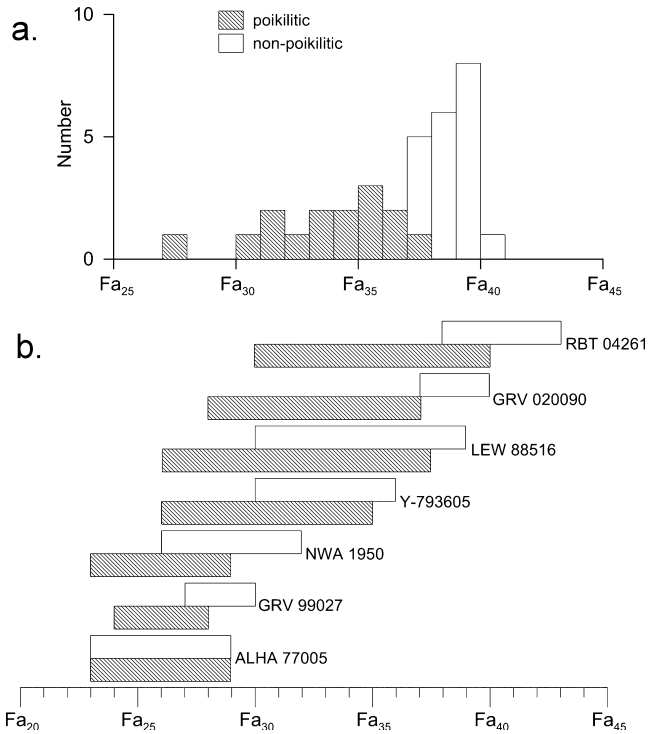

Fig. 3. a) Compositional distribution of olivine in GRV 020090 and b) comparison with those in other "lherzolitic" shergottites. Olivine in poikilitic areas is more magnesian and shows a wider variation than that in nonpoikilitic areas except ALHA77005. Olivine data for the other "lherzolitic" shergottites are from Mikouchi (2005), Mikouchi et al. (2008), and Usui et al. (2010).

Olivine

Like other "lherzolitic" shergottites, olivine in the poikilitic areas is more magnesian ($Fa_{28–37}$) and shows a wider compositional variation than that in the nonpoikilitic area ($Fa_{37–40}$) (Fig. 3a). Olivine compositional range in both areas is largely due to intergrain variations. Within a given grain, olivine is relatively homogeneous. In general, olivine chadacrysts located near the center of the pyroxene oikocryst are more magnesian than those close to the edge. Minor elements in olivine do not show distinct differences between poikilitic and nonpoikilitic areas, although chadacrystic olivines, on average, have slightly higher Cr_2O_3 (0.04 wt%) and lower CaO (0.17 wt%) compared with nonpoikilitic ones (0.01 and 0.23 wt%, respectively).

Olivine in GRV 020090 is slightly more ferroan than those in typical "lherzolitic" shergottites (e.g., LEW 88516), but less ferroan than that of RBT 04261 (e.g., $Fa_{30–43}$, Usui et al. 2010) (Fig. 3b).

Pyroxene

Low-Ca pyroxene in the poikilitic area mainly consists of pigeonite as well as minor orthopyroxene with compositions of $En_{63–72}Fs_{24–28}Wo_{4–11}$. It is also more magnesian than that in the nonpoikilitic area ($En_{57–63}Fs_{26–31}Wo_{7–14}$) (Fig. 4). The pyroxene is

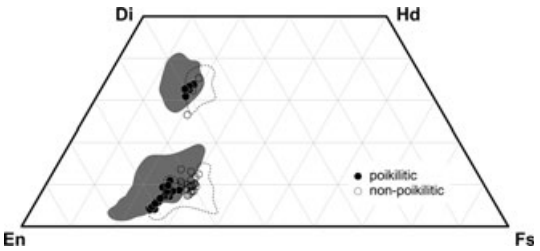

Fig. 4. Pyroxene compositions of GRV 020090 plotted in the En-Wo-Fs system. Ranges of RBT 04262 (dotted line) and "lherzolitic" shergottites (shaded areas) are shown for comparison (Mikouchi and Miyamoto 2000; Mikouchi 2005; Usui et al. 2010).

continuously zoned from Mg-rich cores to relatively Ca-Fe-rich rims. Figure 5 shows variations in minor elements (Ti, Al, and Cr) in pigeonite between poikilitic and nonpoikilitic areas as a function of Fe# [molar Fe/(Fe + Mg)]. The main difference lies in Fe#. Pigeonites in poikilitic areas have Fe# < 0.3, while those in the nonpoikilitic area have Fe# > 0.3. With the increasing of Fe#, TiO_2 and Al_2O_3 of pigeonites in poikilitic areas increase from 0.09 to 0.27 wt% and from 0.46 to 0.8 wt%, respectively, whereas Cr_2O_3 remains almost constant around 0.37 wt%. In the nonpoikilitic area, TiO_2 increases with increasing Fe#, but Al_2O_3 and Cr_2O_3 decrease. These correlations can be explained by element geochemical behaviors. Ti and Al are incompatible in clinopyroxene, whereas Cr is compatible. Al increases in poikilitic pigeonites then decreases in ninpoikilitic ones associated with continuously increasing of Ti. This reflects the onset of plagioclase crystallization, because Al is more compatible in plagioclase than in pigeonite (Bindeman et al. 1998). It is evident that the chemical zoning is of primary magmatic origin, not affected by secondary alteration processes.

High-Ca pyroxenes in both areas have augite compositions and almost overlap, although nonpoikilitic augite ($En_{46–53}Fs_{19–21}Wo_{26–35}$) is slightly more ferroan than poikilitic augite ($En_{47–51}Fs_{17–19}Wo_{31–34}$) (Fig. 4).

Both pigeonite and augite in GRV 020090 are more ferroan than those in typical "lherzolitic" shergottites, but less ferroan than those of RBT 04262 (e.g., $En_{56–72}Fs_{25–35}Wo_{3–14}$ and $En_{44–50}Fs_{17–22}Wo_{30–37}$ for pigeonite and augite, respectively; Usui et al. 2010) (Fig. 4).

Maskelynite

Plagioclase has been entirely transformed into maskelynite by shock. Maskelynite normally shows chemical zoning from $An_{27}Ab_{66}Or_7$ to $An_{53}Ab_{44}Or_2$. Alkali-rich ($An_{1–7}Ab_{36–51}Or_{43–63}$) and silica-excess ($An_{37–62}Ab_{33–55}O_{r4–9}$) maskelynites are also observed (Lin et al. 2008a). In general, Ca decreases and K increases from core to rim within a given grain. A few maskelynite grains show irregular zoning of Ca-rich and alkali-rich areas.

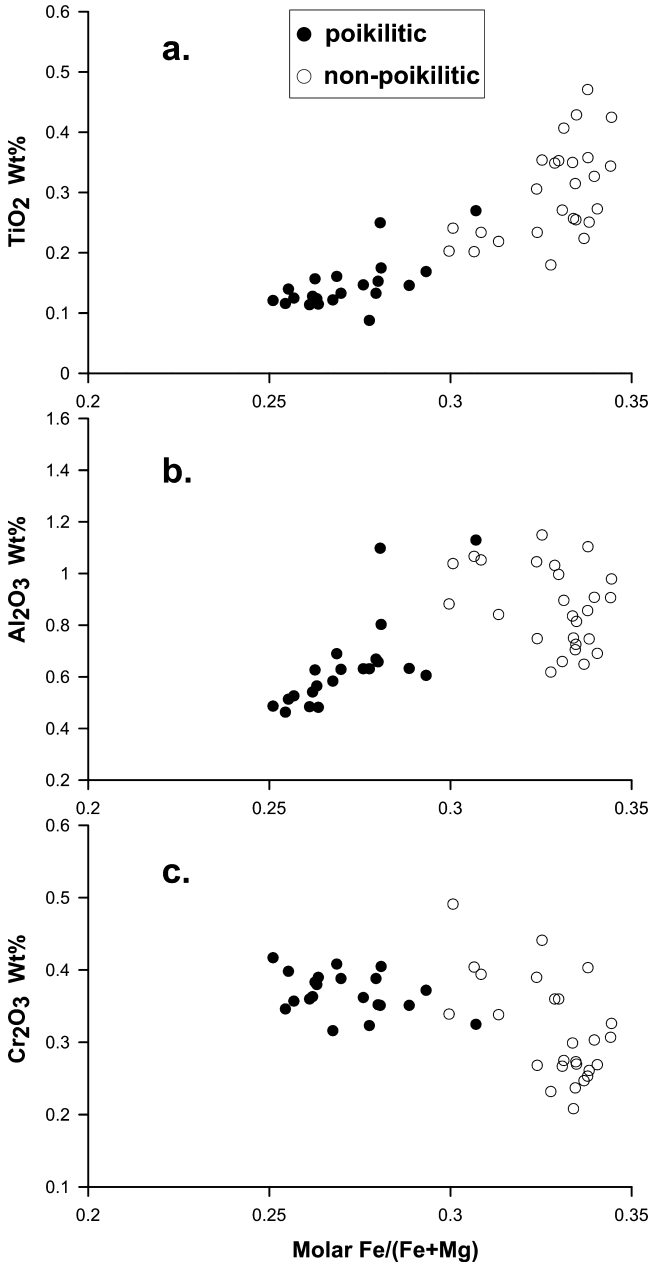

Fig. 5. Variations of a) TiO_2, b) Al_2O_3, and c) Cr_2O_3 versus Fe# [molar Fe/(Fe + Mg)] of low-Ca pyroxenes in GRV 020090. Poikilitic low-Ca pyroxenes have Fe# < 0.3, while nonpoikilitic ones > 0.3.

Maskelynite in GRV 020090 is more alkali-rich than those in typical "lherzolitic" shergottites, but less alkali-rich than that of RBT 04262 (e.g., $An_{22–56}Ab_{42–75}O_r < 10$; Usui et al. 2010) (Fig. 6).

Chromite

Chromite occurs both in poikilitic and in nonpoikilitic areas, but shows different chemical compositions. Chromite grains in poikilitic areas have

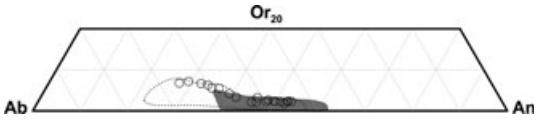

Fig. 6. Maskelynite compositions of GRV 020090 plotted in the Ab-Or-An system. Ranges of RBT 04262 (dotted line) and "lherzolitic" shergottites (shaded area) are shown for comparison (Harvey et al. 1993; Mikouchi 2005; Usui et al. 2010).

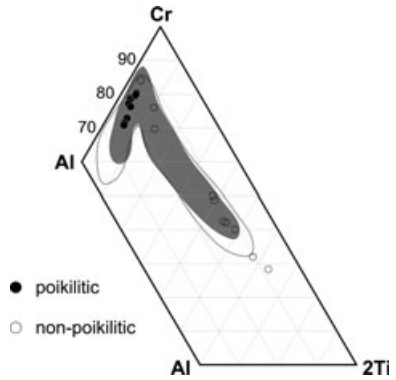

Fig. 7. Al-Cr-2Ti plot of chromite compositions in GRV 020090. Ranges of RBT 04261/2 (dotted line) and "lherzolitic" shergottite Y-793605 (shaded area) are shown for comparison (Ikeda 1997; Usui et al. 2010).

low Ti contents and show a good correlation between Cr and Al (Fig. 7). Their compositions vary from $Chm_{75}Sp_{15}Mt_7Usp_3$ to $Chm_{65}Sp_{22}Mt_9Usp_5$. Previous reports show that chromite compositions are related to their petrographic occurrences: those within olivine chadacrysts are more Al-rich, whereas those within pyroxene oikocrysts are more Cr-rich (Ikeda 1997; Goodrich et al. 2003). Such a trend was not observed in GRV 020090, probably due to sampling (only four chromite grains within one olivine chadacryst were analyzed). In contrast, chromite grains in nonpoikilitic areas show a good correlation between Cr and Ti (Fig. 7), with compositions ranging from $Chm_{77}Sp_{12}Mt_8Usp_3$ to $Chm_{23}Sp_7Mt_{20}Usp_{50}$. Some chromite grains are zoned. The cores are similar to those of the most Cr-rich chromites in poikilitic areas and Ti and Fe smoothly increase toward the edge.

In the Mg# [molar Mg/(Mg + Fe)] versus Cr# [molar Cr/(Cr + 2Ti + Al)] diagram (Fig. 8), chromites in nonpoikilitic areas show a positive correlation, in accordance with a typical magmatic trend in basalts (Barnes and Roeder 2001). Chromites in poikilitic olivine share similar Cr# to those in pyroxene, but exhibit lower Mg#, suggesting that chromites in olivine may have been affected by higher degrees of Fe/Mg re-equilibration with their hosts (Goodrich et al. 2003). This effect can be explained by higher diffusion rates in olivine than in pyroxene.

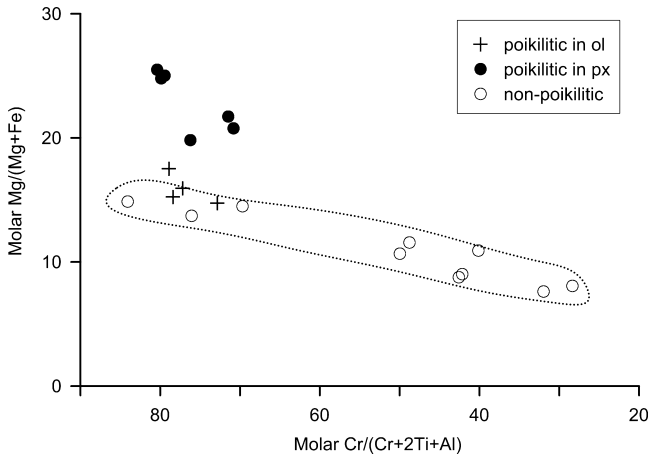

Fig. 8. Mg# [molar Mg/(Mg + Fe)] versus Cr# [molar Cr/(Cr + 2Ti + Al)] of chromite in chadacrystic olivine, oikocrystic pyroxene, and nonpoikilitic areas.

Both Cr-Al correlation in poikilitic chromite and Cr-Ti correlation in nonpoikilitic chromite are consistent with those in other "lherzolitic" shergottites, but GRV 020090 chromite has lower Mg# (8–26) and higher Usp components (3–50) than in typical "lherzolitic" shergottites (e.g., 16–33 and 2–35 for Mg# and Usp components in GRV 99027, respectively) (Lin et al. 2005). Moreover, $Fe^{3+}/\sum Fe$ ratios of chromite (16–23) in GRV 020090 are significantly higher than those in GRV 99027 (5–12, Lin et al. 2005), suggesting a higher oxygen fugacity during crystallization (Herd et al. 2002). In comparison, GRV 020090 chromite has a similar Mg# to that of RBT 04261/2 (approximately 10–30) (Usui et al. 2010).

Minor Phases

Merrillite has a relatively homogeneous chemical composition and contains 2 wt% Na_2O, 45.9 wt% P_2O_5, and 47.2 wt% CaO. Rare apatite was also observed. Ilmenite usually occurs with chromite, occasionally with baddeleyite. Their representative analyses are present in Table 2.

REE Compositions

REE analyses were carried out in situ in olivine, pigeonite, augite, maskelynite, merrillite, and fusion crust. Representative results are reported in Table 3.

Olivine

LREE abundances in olivine are usually below the detection limit. As shown in Fig. 9a, the CI-normalized REE abundances increase gradually from Gd ($0.1 \times$ CI) to Lu ($1 \times$ CI). Olivine in poikilitic area is indistinguishable from that in nonpoikilitic area. Within analytical uncertainties, GRV 020090 olivine has essentially identical HREE abundances to those of RBT 04261/2 and typical "lherzolitic" shergottites.

Pyroxene

Pyroxenes in GRV 020090 show more than an order of magnitude variation in their REE concentrations (Figs. 9b and 9c). REE abundances of pigeonite are significantly lower than those of augite. The REE pattern for pigeonite is LREE-depleted and its slope is steeper [$(Yb/La)_{CI} \sim 34$] than that for augite [$(Yb/La)_{CI} \sim 11$]. The core of pigeonite oikocryst has the lowest REE abundances with LREE below the detection limit, whereas augite in nonpoikilitic areas has the highest REE concentrations. Poikilitic augite has negative Eu anomalies (Eu/Eu* = 0.3–0.4, where Eu is the measured chondrite-normalized value and Eu* is the value interpolated between Sm and Gd), indicating cocrystallization with plagioclase. No apparent Ce anomalies were observed. Both pigeonite and augite in GRV 020090 exhibit REE patterns similar to those in the enriched basaltic shergottites ($[Yb/La]_{CI}$ = 24–33 and 14 for Shergotty pigeonite and augite, respectively; Wadhwa et al. 1994) and those in RBT 04261/2 ($[Yb/La]_{CI}$ approximately 25 and 9 for pigeonite and augite, respectively; Usui et al. 2010), but distinct from those in typical "lherzolitic" shergottites ($[Yb/La]_{CI}$ = 60–100 and 40 for LEW 88516 pigeonite and augite, respectively; Harvey et al. 1993).

Maskelynite

The REE pattern for maskelynite is LREE-enriched with a large positive Eu anomaly (Fig. 9d). GRV 020090 maskelynite has relatively higher REE (La approximately $0.8 \times$ CI) than those of typical "lherzolitic" shergottites (La approximately $0.3 \times$ CI for LEW 88516; Wadhwa et al. 1994) and the enriched basaltic shergottite (La approximately $0.4 \times$ CI for Shergotty; Wadhwa et al. 1994). In comparison, GRV 020090 maskelynite has similar REE concentrations to that of RBT 04261/2 (La approximately $0.8 \times$ CI) (Usui et al. 2010).

Merrillite

The main phosphate phase in GRV 020090 is merrillite. Apatite is found in trace amounts. Among minerals analyzed, merrillite is the major REE carrier (La approximately 572–841 $\times$ CI). Figure 10a shows average REE abundances of merrillite in GRV 020090. Its REE pattern is relatively flat with $(Gd/La)_{CI}$ approximately 1, and essentially resembles those of merrillite in RBT 04261 and geochemically enriched basaltic shergottite Shergotty (Lundberg et al. 1988; Usui et al. 2010). In contrast, merrillite in typical "lherzolitic" shergottites is relatively LREE-depleted with lower REE concentrations (La approximately 180 $\times$ CI for LEW 88516 and GRV 99027) (Harvey et al. 1993; Hsu et al. 2004; Lin et al. 2005).

Table 3. Representative REE abundances (ppm) of minerals and fusion crust in GRV 020090. Errors are 1σ on counting statistics only.

	Poikilitic area					Nonpoikilitic area					
	Olivine	Pigeonite (c)	Pigeonite (r)	Augite (c)	Augite (r)	Olivine	Pigeonite	Augite	Maskelynite	Merrillite	Fusion crust
La	b.d.	b.d.	b.d.	0.071 ± 0.011	0.145 ± 0.013	b.d.	0.031 ± 0.006	0.161 ± 0.014	0.190 ± 0.027	157.4 ± 1.6	0.949 ± 0.035
Ce	b.d.	b.d.	b.d.	0.396 ± 0.021	0.594 ± 0.027	b.d.	0.102 ± 0.012	0.736 ± 0.027	0.381 ± 0.031	359.2 ± 3.4	2.43 ± 0.06
Pr	b.d.	b.d.	b.d.	0.096 ± 0.012	0.151 ± 0.014	b.d.	0.026 ± 0.006	0.160 ± 0.013	0.049 ± 0.012	55.6 ± 0.7	0.360 ± 0.018
Nd	b.d.	b.d.	0.079 ± 0.038	0.621 ± 0.085	1.19 ± 0.12	b.d.	0.288 ± 0.046	1.28 ± 0.11	0.233 ± 0.074	276.0 ± 3.3	1.81 ± 0.14
Sm	b.d.	b.d.	b.d.	0.463 ± 0.060	0.614 ± 0.075	b.d.	0.161 ± 0.043	0.707 ± 0.075	b.d.	99.0 ± 1.4	0.815 ± 0.082
Eu	b.d.	0.008 ± 0.003	0.023 ± 0.009	0.155 ± 0.017	0.238 ± 0.026	b.d.	0.085 ± 0.015	0.222 ± 0.020	0.605 ± 0.057	28.2 ± 0.4	0.272 ± 0.023
Gd	0.025 ± 0.022	0.047 ± 0.012	0.149 ± 0.040	0.796 ± 0.071	1.42 ± 0.11	b.d.	0.459 ± 0.059	1.53 ± 0.10	b.d.	156.6 ± 2.2	1.13 ± 0.09
Tb	0.002 ± 0.002	0.012 ± 0.004	0.037 ± 0.007	0.206 ± 0.014	0.301 ± 0.018	0.004 ± 0.003	0.130 ± 0.014	0.329 ± 0.021	b.d.	27.9 ± 0.3	0.194 ± 0.015
Dy	0.022 ± 0.013	0.121 ± 0.029	0.282 ± 0.035	1.18 ± 0.06	2.06 ± 0.10	0.028 ± 0.014	0.976 ± 0.066	2.41 ± 0.11	0.043 ± 0.013	181.0 ± 2.0	1.56 ± 0.09
Ho	0.013 ± 0.004	0.030 ± 0.005	0.054 ± 0.007	0.249 ± 0.018	0.433 ± 0.022	0.006 ± 0.003	0.206 ± 0.016	0.503 ± 0.022	b.d.	36.1 ± 0.4	0.302 ± 0.019
Er	0.048 ± 0.013	0.099 ± 0.017	0.167 ± 0.021	0.786 ± 0.047	1.24 ± 0.06	0.044 ± 0.012	0.783 ± 0.051	1.38 ± 0.07	0.028 ± 0.012	101.9 ± 1.1	0.867 ± 0.062
Tm	0.011 ± 0.004	0.021 ± 0.005	0.027 ± 0.005	0.112 ± 0.010	0.170 ± 0.013	0.017 ± 0.005	0.112 ± 0.010	0.182 ± 0.011	0.003 ± 0.001	13.7 ± 0.2	0.116 ± 0.010
Yb	0.098 ± 0.027	0.112 ± 0.030	0.271 ± 0.040	0.614 ± 0.059	1.09 ± 0.08	0.133 ± 0.030	0.760 ± 0.064	1.24 ± 0.09	0.008 ± 0.005	82.7 ± 1.2	0.715 ± 0.079
Lu	0.027 ± 0.006	0.028 ± 0.006	0.044 ± 0.007	0.096 ± 0.008	0.160 ± 0.013	0.034 ± 0.006	0.096 ± 0.009	0.176 ± 0.013	b.d.	11.8 ± 0.2	0.123 ± 0.011

b.d. = below detection limit.

"c" and "r" refer to the core and rim REE abundances of pyroxene.

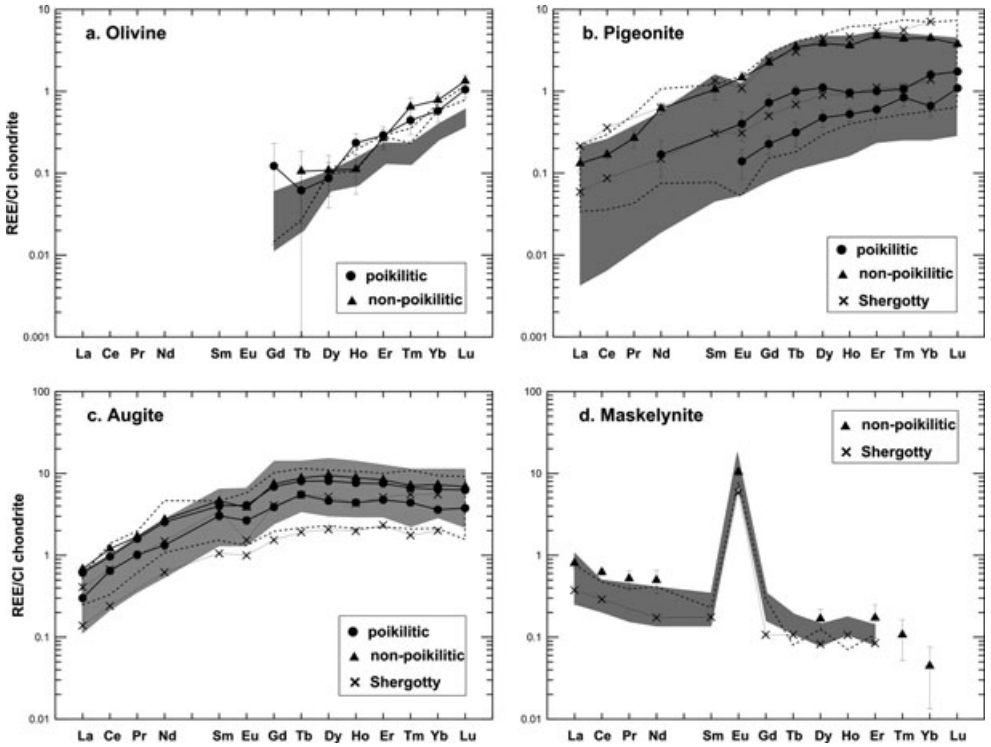

Fig. 9. CI-normalized REE abundances of a) olivine, b) pigeonite, c) augite, and d) maskelynite in GRV 020090. Shaded areas show REE abundances in other "lherzolitic" shergottites (ALHA77005, LEW 88516, Y-793605, and GRV 99027) (Harvey et al. 1993; Wadhwa et al. 1994, 1999; Lin et al. 2005). RBT 04261/2 (dotted line) and basaltic shergottite Shergotty are also shown for comparison (Wadhwa et al. 1994; Usui et al. 2010). Error bars indicate uncertainties ($\pm 1\sigma$) due to counting statistics only.

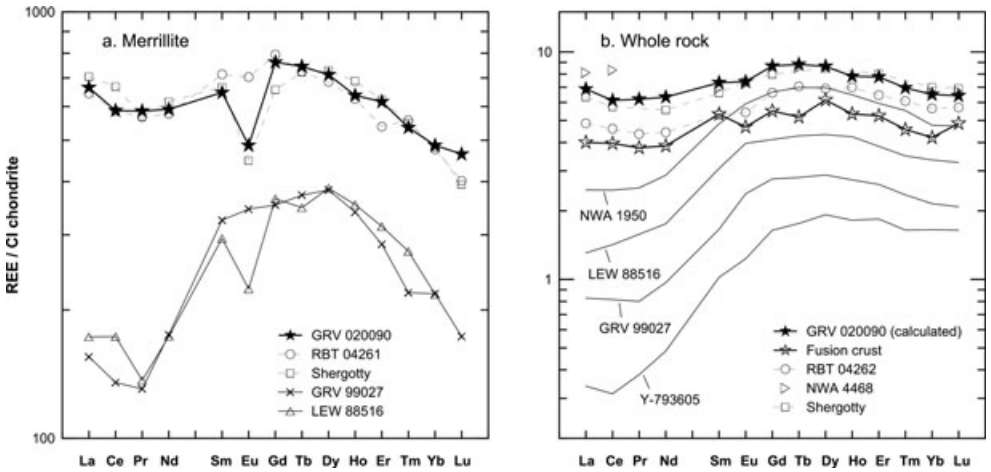

Fig. 10. CI-normalized REE abundances of a) merrillite and b) whole rock. Merrillite as well as the whole-rock (calculated) and the fusion crust of GRV 020090 show similar LREE-enriched patterns to those of RBT 04261/2 (Anand et al. 2008; Usui et al. 2010), NWA 4468 (Irving et al. 2007), and basaltic shergottite Shergotty (Shih et al. 1982; Lundberg et al. 1988), but distinct from those of "lherzolitic" shergottites NWA 1950 (Gillet et al. 2005), LEW 88516 (Dreibus et al. 1992; Harvey et al. 1993), GRV 99027 (Lin et al. 2005, 2008b) and Y-793605 (Ebihara et al. 1997).

Fusion Crust

The REE pattern of the fusion crust is relatively flat (approximately $4 \times$ CI) and parallel to that of the calculated whole-rock of GRV 020090 (see REE Budget in the Discussion section) (Fig. 10b).

Baddeleyite U-Pb Age

A total of 11 baddeleyite grains were found in the section of GRV 020090-1. They are very small, ranging from 3 to 22 μm in the largest dimension. Only six

Table 4. U-Th-Pb isotopic analysis of baddeleyite in GRV 020090.

Sample spot	U (ppm)	Th (ppm)	Th/U	f_{206}[a] (%)	$^{238}U/^{206}Pb$	±1σ (%)	$^{207}Pb/^{206}Pb$	±1σ (%)	^{207}Pb-corr[b] age (Ma)	±1σ (Ma)
badd-2@1	129	5.44	0.042	88	4.43	10.8	0.7606	4.9	179	78
badd-2@2	76	7.26	0.095	80	6.08	10.3	0.6944	6.8	215	69
badd-3@1	217	2.76	0.013	69	9.25	8.4	0.6105	5.4	212	36
badd-3@2	149	3.09	0.021	71	9.13	6.4	0.6227	5.3	205	34
badd-3@3	130	1.78	0.014	40	19.54	5.3	0.3762	5.5	194	14
badd-3@4	103	1.71	0.017	69	9.25	8.1	0.6082	5.2	214	35
badd-4@1	35	0.51	0.014	20	23.58	10.0	0.2128	14.3	215	24
badd-4@2	41	0.82	0.020	45	21.38	10.3	0.4113	11.0	165	24
badd-4@3	37	0.47	0.013	15	31.48	9.9	0.1706	15.1	172	18
badd-4@4	42	0.75	0.018	49	22.86	10.2	0.4494	10.6	142	22
badd-4@5	41	0.45	0.011	32	23.24	9.1	0.3103	10.3	186	20
badd-5@1	110	0.63	0.006	6.0	28.92	6.1	0.0988	11.4	206	13
badd-5@2	113	0.92	0.008	3.9	29.48	6.1	0.0817	12.0	207	13
badd-6@1	95	0.83	0.009	29	22.52	6.8	0.2864	11.1	200	17
badd-6@2	64	0.61	0.010	57	15.53	10.2	0.5156	9.4	175	31
badd-7@1	37	0.36	0.010	40	23.79	11.3	0.3709	12.9	162	24
badd-7@2	45	0.31	0.007	34	23.94	11.3	0.3246	13.0	176	24
badd-7@3	59	0.50	0.008	46	16.17	9.0	0.4228	9.1	212	27

[a] f_{206} is the percentage of common ^{206}Pb in total ^{206}Pb.
[b] Common Pb compositions are determined by the *y*-axis intersection of the Tera-Wasserburg plot.

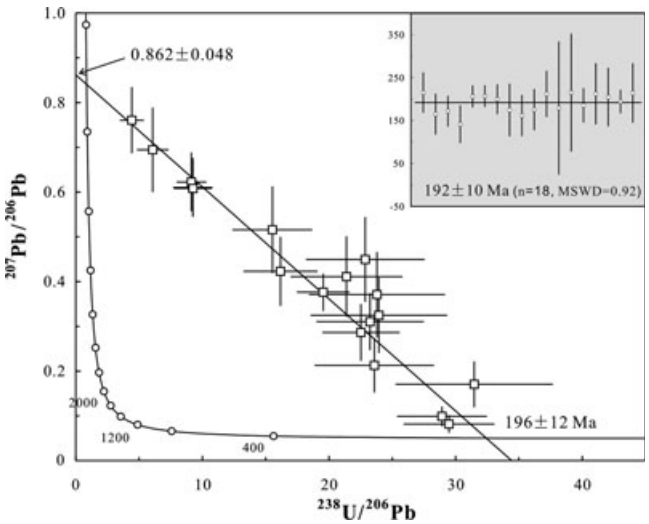

Fig. 11. U-Pb isotopic systematics of baddeleyite on the Tera-Wasserburg concordia diagram. Eighteen analysis points without common lead correction distribute along a mixing line whose end-members are the radiogenic lead on the concordia curve (196 ± 12 Ma) and the common lead at zero $^{238}U/^{206}Pb$ ($^{207}Pb/^{206}Pb$ = 0.862 ± 0.048). With this ratio as the best estimate of common lead composition, the ^{207}Pb-corrected $^{206}Pb/^{238}U$ ages yield a weighted average of 192 ± 10 Ma (the inset). Errors quoted are 2σ.

baddeleyite grains (> 5 μm) were chosen for in situ U-Th-Pb isotopic analyses. As listed in Table 4, 18 analyses display highly variable uranium contents ranging from 35 to 217 ppm. The average uranium concentration in baddeleyite is 85 ppm, similar to that of RBT 04261/2 (Hays et al. 2011; Niihara 2011). Thorium concentrations are very low (0.31–7.26 ppm), and thorium/uranium ratios vary from 0.006 to 0.095. The ^{207}Pb-based f_{206} values vary from 4% to 88%, indicating highly variable proportions of common lead. For cogenetic samples that have had no later lead loss, the total $^{238}U/^{206}Pb$ and $^{207}Pb/^{206}Pb$ data without common lead correction will lie, within measurement error, on a mixing line between the purely radiogenic lead and the common lead (Tera and Wasserburg 1972). On the Tera-Wasserburg concordia (Fig. 11), a widespread distribution of data yields a good linear regression line. It has a lower intercept with the concordia curve at 196 ± 12 Ma, and an upper intercept on the *y*-axis at 0.862 ± 0.048 (2σ), which is close to the $^{207}Pb/^{206}Pb$ ratio of modern terrestrial lead ($^{207}Pb/^{206}Pb$ = 0.836) (Stacey and Kramers 1975) or those of laboratory blank lead ($^{207}Pb/^{206}Pb$ = 0.826–0.856) (Chen and Wasserburg 1986; Bouvier et al. 2005). With the upper intercept employed as the common lead composition, ^{207}Pb-corrected $^{206}Pb/^{238}U$ ages result in a weighted average of 192 ± 10 (2σ) Ma.

DISCUSSION

Crystallization Sequence

Like other "lherzolitic" shergottites, GRV 020090 is a cumulate. The rounded or subhedral outlines of olivine chadacrysts suggest partial absorption by melt, in agreement with the origin of cumulus mineral. GRV 020090 exhibits two distinct lithologies: poikilitic and

nonpoikilitic, indicating two different crystallization stages. Olivine and pyroxene in the poikilitic areas show higher Mg# than those in the nonpoikilitic areas (Figs. 3a and 4), and poikilitic pyroxenes have distinctly lower REE abundances than nonpoikilitic ones (Fig. 9b). It is clear that the poikilitic lithology formed earlier than the nonpoikilitic one. As shown in Fig. 9c, poikilitic augites have negative Eu anomalies indicative of cocrystallization with plagioclase, suggesting that in the final stage of poikilitic lithology formation, plagioclase in the nonpoikilitic area began to crystallize. In the nonpoikilitic area, pyroxene intergrows with plagioclase indicating cocrystallization (Fig. 2b). The inferred crystallization sequence of minerals in GRV 020090 was as follows: chromite → olivine → poikilitic low-Ca pyroxene → poikilitic high-Ca pyroxene, nonpoikilitic pyroxenes (pigeonite and augite) and plagioclase → merrillite. Olivine grains in nonpoikilitic areas are more ferroan and show a narrower variation than that in poikilitic areas (Fig. 3a), suggesting that they experienced re-equilibration with intercumulus melt after accumulation. In contrast, olivine in poikilitic areas is surrounded by pyroxene oikocrysts and did not exchange with a melt. Chromite might have experienced a similar process.

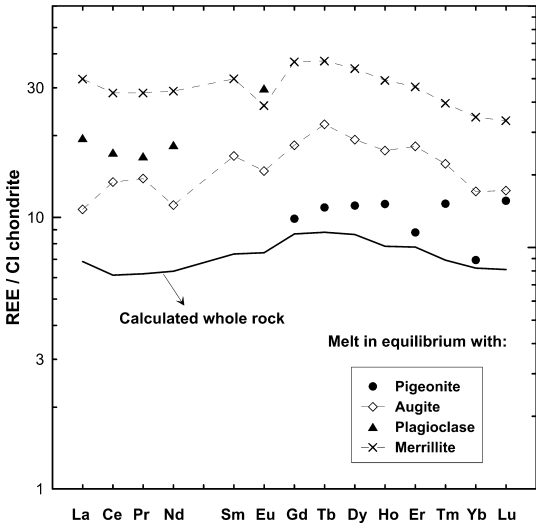

Fig. 12. Calculated CI-normalized REE patterns of melts in equilibrium with poikilitic pigeonite and augite, as well as nonpoikilitic plagioclase (now maskelynite) and merrillite. The solid line shows the calculated whole-rock REE in this work. The mineral/liquid partition coefficients are taken from Lundberg et al. (1990). Large uncertainties of partition coefficients for Tm, Yb, and Lu in pigeonite may result in some irregularities of REE pattern.

REE Budget

As can be seen in Table 3, major phases such as pyroxene, olivine, and maskelynite contain very low REE contents, whereas merrillite, although a minor phase, has the highest REE concentrations. Other accessory phases, such as opaque minerals, are essentially devoid of REE (Lundberg et al. 1988). The whole-rock REE abundances of GRV 020090 are mainly controlled by merrillite. Using the modal abundance and average analyses of individual minerals (Tables 1 and 3), we estimated the whole-rock REE abundances. It is obvious that the absolute REE concentrations of GRV 020090 whole rock are less well constrained due to the heterogeneous distribution of merrillite. Yet, the relative REE abundances, e.g., $(Yb/La)_{CI}$, are much more reliable. The calculated whole-rock REE pattern of GRV 020090 shows a good agreement with geochemically enriched basaltic shergottite Shergotty, and almost parallels to RBT 04262 and NWA 4468 (Shih et al. 1982; Irving et al. 2007; Anand et al. 2008). This LREE-enriched pattern is significantly different from those of relatively LREE-depleted "lherzolitic" shergottites (NWA 1950, LEW 88516, GRV 99027, and Y-793605) (Fig. 10b).

Parent Melt REE Compositions

The REE concentrations of melts in equilibrium with minerals can be estimated using REE compositions of minerals and mineral/liquid partition coefficients. As REE are incompatible in pyroxenes and plagioclase, we use the lowest REE abundances in these phases to determine the REE of melts from which these phases crystallized. In contrast, REE are compatible in merrillite, and we use the highest REE concentrations present in this phase. Partition coefficients used here are all from Tables 3 and 4 in Lundberg et al. (1990).

Figure 12 shows REE abundances of melts in equilibrium with poikilitic pigeonite and augite, nonpoikilitic plagioclase, and merrillite. They increase from that of the poikilitic pigeonite core to augite, to plagioclase, and then to merrillite. This is generally consistent with the crystallization sequence in GRV 020090. Olivine and chromite were the first phases crystallized from the parent melt. They incorporated negligible REE and left with a melt with elevated REE abundances. As the crystallization proceeded, pyroxene and plagioclase began to crystallize from the melt. As REE are also incompatible in pyroxene and plagioclase, the melt became progressively enriched in REE. During the final stage of crystallization, merrillite crystallized from a melt with even higher REE than the initial parental melt (the estimated whole rock). These observations strongly suggest that all mineral phases in GRV 020090 originated from a single parent melt and experienced fractional crystallization in a closed magmatic system. This is also supported by the coherent

Table 5. Calculated temperature and oxygen fugacity of GRV 020090.

	Olivine	Chromite	Pigeonite
SiO_2	37.31	0.24	54.69
TiO_2	0.03	1.30	0.12
Al_2O_3	0.08	7.12	0.46
Cr_2O_3	0.05	53.56	0.35
FeO	27.56	29.66	15.50
MnO	0.56	0.53	0.51
MgO	33.69	5.69	25.48
CaO	0.15	b.d.	2.03
Na_2O	0.04	b.d.	0.07
K_2O	0.01	b.d.	0.03
Total	99.5	98.4	99.2
Si	1.003	0.008	1.996
Ti	0.001	0.034	0.003
Al	0.003	0.294	0.020
Cr	0.001	1.484	0.010
Fe^{3+}	0.000	0.143	0.000
Fe^{2+}	0.620	0.726	0.473
Mn	0.013	0.009	0.016
Mg	1.350	0.297	1.386
Ca	0.004	0.000	0.079
Na	0.002	0.000	0.005
K	0.000	0.000	0.001
Total	2.996	2.997	3.989
T (°C)	920 ± 50[a]		
fO_2 (log unit)	QFM−1.41 ± 0.04[b]		

b.d. = below detection limit.
[a]Calculation is after Sack and Ghiorso (1991).
[b]Calculation is after Wood et al. (1990).

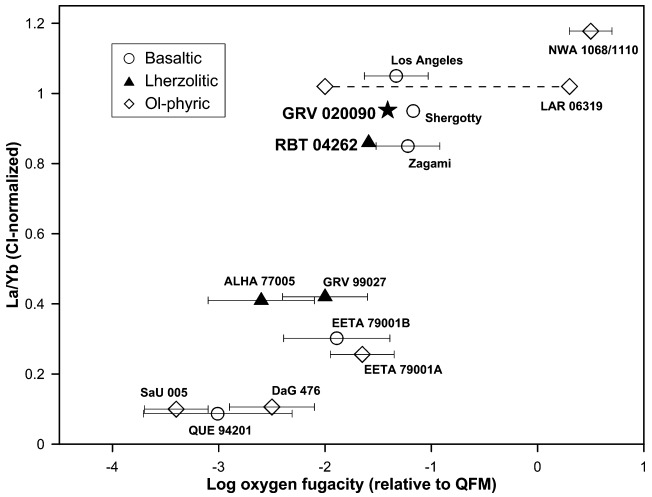

Fig. 13. CI-normalized whole rock La/Yb ratio versus oxygen fugacities for GRV 020090 (filled star) and other shergottites. The whole rock La/Yb ratio of GRV 020090 is calculated using the fusion crust data. Basaltic shergottites: QUE 94201, EETA 79001B, Zagami and Shergotty (Lodders 1998; Herd et al. 2001), Los Angeles (Rubin et al. 2000; Herd et al. 2001); "Lherzolitic" shergottites: RBT 04262 (Anand et al. 2008; Usui et al. 2010), GRV 99027 (Lin et al. 2005), ALHA77005 (Lodders 1998; Goodrich et al. 2003); Olivine-phyric shergottites: SaU 005 (Dreibus et al. 2000; Herd 2003), DaG 476 (Zipfel et al. 2000; Herd 2003), EETA 79001A (Lodders 1998; Herd et al. 2001), LAR 06319 (Peslier et al. 2010), NWA 1068/1110 (Barrat et al. 2002; Herd 2006). Dashed line shows oxygen fugacity ranges of LAR 06319 during crystallization (Peslier et al. 2010). Oxygen fugacity of the early assemblage in NWA 1068/1110 is not shown because of its xenocrystic origin (Herd 2006).

trends of minor elements observed in poikilitic and nonpoikilitic pigeonites (Fig. 5).

Temperature and Oxygen Fugacity

Using the two-pyroxene thermometer (Lindsley 1983), coexisting pigeonite ($En_{64}Fs_{25}Wo_{11}$) and augite ($En_{48}Fs_{19}Wo_{34}$) in poikilitic areas yield a subsolidus equilibration temperature of 1100–1200 °C. Oxygen fugacity (fO_2) of the parent magma of GRV 020090 can be determined using an olivine-chromite-pigeonite barometer (Table 5). We assume that GRV 020090 crystallized at near surface conditions with approximately 1 bar, as the oxygen fugacity is insignificantly affected by pressure (Wood et al. 1990). Coexisting olivine-chromite-pigeonite grains yield a subsolidus equilibration temperature (920 ± 50 °C) and an oxygen fugacity ($\log fO_2$ = QFM−1.41 ± 0.04). The pigeonite Eu-oxybarometer can be applied to calculate the earliest oxygen fugacity of the melt (McCanta et al. 2004). However, due to large uncertainties and the extremely low REE concentrations in the oikocrystic pigeonite, calculation does not yield any reasonable fO_2 value. The equilibration temperature estimated by the two-pyroxene thermometer (1100–1200 °C) is significantly higher than that between olivine and chromite (920 ± 50 °C). This was also previously noted in other "lherzolitic" shergottites (Lin et al. 2005; Usui et al. 2010). It can be explained by the fact that cation diffusion rates (e.g., Fe-Mg) between olivine and chromite are much faster than that (e.g., Fe-Mg-Ca) in pyroxenes (Fabriès 1979).

The oxygen fugacities of shergottites correlate well with their whole-rock La/Yb ratios, forming a trend from reduced and LREE-depleted (e.g., QUE 94201) to oxidized and LREE-enriched shergottites (e.g., NWA 1068/1110) (Fig. 13). GRV 020090 falls on the oxidized and enriched end of this trend, close to enriched basaltic shergottite Shergotty. This characteristic strongly supports that GRV 020090 represents the crystallization product of a melt from an oxidized and enriched mantle reservoir. In particular, GRV 020090 is a new enriched "lherzolitic" shergottite, different from typical "lherzolitic" shergottites with an intermediate geochemical signature except RBT 04261/2 (Fig. 13).

Two competing models have been proposed to explain the correlation between oxygen fugacity and REE pattern in shergottites: assimilation of enriched, oxidized crust by depleted, reduced mantle magmas (Wadhwa 2001; Herd et al. 2002), or mixing of distinct mantle reservoirs produced by either crystallization of a magma ocean (Borg and Draper 2003) or fluid-induced metasomatism (Treiman 2003). The closed-system behavior of GRV 020090 does not appear to support the assimilation model (Hui et al. 2011). The lack of correlation between major and trace element abundances in shergottites also confirms this supposition (Symes et al. 2008).

Crystallization Age

Mineral isochron ages of shergottites using different long-lived radiogenic systematics (^{87}Rb-^{87}Sr, ^{147}Sm-^{143}Nd, ^{176}Lu-^{176}Hf, U-Pb) were reported by numerous workers (Nyquist et al. 2001; Borg and Drake 2005). As a whole, formation of shergottites spans an age range from 150 to 575 Ma. Geochemically depleted shergottites are the oldest (330–575 Ma); the enriched are the youngest (150–230 Ma); and intermediate ones cluster around 180 Ma except NWA 1460/480 approximately 346 Ma (Symes et al. 2008; Nyquist et al. 2009). However, young crystallization ages of shergottites have been challenged recently. Bouvier et al. (2005) reported an approximately 4.1 Ga ^{207}Pb-^{206}Pb age of leached bulk rock and mineral separate fractions of Zagami and argued that lithosphere of Mars is extremely old. They suggested that the young ages for shergottites might result from resetting events such as fluid–rock interaction or shock metamorphism during impact (Bouvier et al. 2008, 2009).

To evaluate the effects of secondary metamorphic processes on the crystallization age of shergottites, we applied SIMS to make in situ measurements of U-Pb ages in baddeleyite. Baddeleyite (ZrO_2) is an ideal candidate for U-Pb dating of lunar and Martian meteorites. It can take up abundant U, exclude initial common Pb, and is resistant to metamorphic processes. In this work, the weighted average of the eighteen ^{206}Pb/^{238}U ages obtained for GRV 020090 baddeleyites is 192 ± 10 (2σ) Ma. This age is in excellent agreement with those of other geochemically enriched shergottites (Misawa and Yamaguchi 2007; Hays et al. 2011; Niihara 2011).

We believe that this age is the true crystallization age of GRV 020090 for the following two reasons (1) the origin of baddeleyite. Baddeleyite grains in GRV 020090 are often associated with ilmenite, rarely with maskelynite. High-pressure/temperature polymorph or silica glass was not observed close to these grains. Baddeleyite surrounded by impact melt was also not observed. These occurrences suggest that baddeleyite grains formed as late-stage minerals during the magma crystallization, rather than from the decomposition of zircon ($ZrSiO_4 \rightarrow ZrO_2 + SiO_2$) (El Goresy 1965). In addition, decomposition of zircon requires peak shock pressures >60 GPa and post-shock temperatures >1600 °C (Wittmann et al. 2006). This pressure largely exceeds the observed shock pressure range for shergottites (30–45 GPa) (Nyquist et al. 2001). (2) The shock metamorphism issue. The *P–T* phase diagram (Ohtaka et al. 2001) shows that baddeleyite is monoclinic under igneous crystallization conditions (T < 1000 °C, P < 4 GPa). When pressure exceeds 4 GPa, baddeleyite transforms into an orthorhombic phase (ortho I) below 600 °C and a tetragonal phase above 600 °C; at approximately 14 GPa, both phases transform into another orthorhombic phase (ortho II). Bouvier et al. (2008) argued that successive phase changes of baddeleyite would result in disturbance of U-Pb systematics. However, the transmission electron microscope (TEM) analysis of baddeleyite in the NWA 3171 shergottite demonstrated that baddeleyite retains its low-pressure crystal structure, although subjected to peak shock pressures of 30–35 GPa (Herd et al. 2010). The Raman spectra analysis also demonstrated that shock metamorphism does not result in polymorphic phase transformations (Niihara 2011). Most importantly, shock recovery experiments on Phalaborwa baddeleyite indicate that shock pressures up to 57 GPa do not disturb U-Pb isotopic systematics (Niihara et al. 2009). Therefore, the U-Pb age of 192 ± 10 (2σ) Ma determined on baddeleyite would not be affected by shock metamorphism and represent the true crystallization age of GRV 020090. Recent dating work by Rb-Sr, Sm-Nd, Ar-Ar, and Lu-Hf techniques of NWA 1460 and LAR 06319 also confirmed that shergottites have young igneous ages (Nyquist et al. 2009; Shafer et al. 2010). As for the ancient ^{207}Pb-^{206}Pb age reported by Bouvier et al. (2005, 2008, 2009), Gaffney et al. (2007) interpreted it as the result of incomplete removal of modern terrestrial Pb during leaching.

In summary, the young ages rather than ancient ages (>4 Ga) appear to represent the crystallization of Martian surface lava flow. This view is also supported by recent crater counts on the basis of updated high-resolution imagery, suggesting that young surface regions are much more widespread on Mars than previously thought (Neukum et al. 2010).

GRV 020090 and RBT 04261/2: Enriched "Lherzolitic" Shergottites

As described above, GRV 020090 shows many similarities to RBT 04261/2, which were collected from

Roberts Massif in Antarctica in 2004. RBT 04261/2 were initially classified as olivine-phyric shergottites (Satterwhite and Righter 2007). Detailed petrographic and geochemical studies indicate that they are enriched "lherzolitic" shergottites (Anand et al. 2008; Mikouchi et al. 2008; Usui et al. 2010). Both GRV 020090 and RBT 04261/2 have similar modal abundances of major minerals (Table 1). Their olivine and pyroxene are slightly more ferroan than those of typical "lherzolitic" shergottites (Figs. 3 and 4), and maskelynite is more alkali-rich (Fig. 6). Minerals and the whole rocks of both meteorites have similar REE abundances and exhibit an LREE-enriched pattern and a high oxygen fugacity (Figs. 9, 10, and 13). The crystallization age of GRV 020090 is also indistinguishable from that of RBT 04261 (approximately 200 Ma; Niihara 2011). It is clear that GRV 020090 is petrologically and geochemically closely related to RBT 04261/2, and probably launch paired. They would have been ejected from the same igneous unit on Mars during an impact event. Further ejection age measurements are needed to confirm their relationship.

The composition of GRV 020090 fusion crust [CaO 5.65 wt% and Mg/(Mg + Fe) ratio ~ 0.64], along with that of RBT 04261/2, plots in the permafic field on the compositional diagram presented in Irving et al. (2010). In contrast, typical "lherzolitic" shergottites (ALHA77005, Y-793605, LEW 88516, GRV 99027) are ultramafic except NWA 1950. More recently discovered shergottite NWA 4468 is very similar to both GRV 020090 and RBT 04261/2 (Irving et al. 2007). Compared with typical "lherzolitic" shergottites, these three meteorites contain a high abundance of maskelynite (approximately 20 vol%), and have minerals relatively Fe-enriched. It may reflect the petrographic diversities among "lherzolitic" shergottites. These enriched "lherzolitic" shergottites share many trace element and isotopic characteristics with other Martian meteorites such as Shergotty, Zagami, Los Angeles, NWA 1068/1110, and LAR 06319. The MELTS algorithm suggested that these enriched shergottites could be related to a similar mantle source region by variable degrees of fractional crystallization (Borg et al. 2008; Marks et al. 2010).

CONCLUSIONS

GRV 020090 is a "lherzolitic" shergottite collected in the Grove Mountains, Antarctica. It comprises two petrographic lithologies: a poikilitic area consisting of pyroxene oikocrysts with subhedral olivine and chromite inclusions, and a nonpoikilitic area consisting of olivine, pyroxene with interstitial maskelynite along with minor amounts of chromite and merrillite. The inferred crystallization sequence is: chromite → olivine → poikilitic low-Ca pyroxene → poikilitic high-Ca pyroxene, nonpoikilitic pyroxenes (pigeonite and augite) and plagioclase → merrillite. Compared with typical "lherzolitic" shergottites, GRV 020090 contains more maskelynite, which is related to the higher proportion of the nonpoikilitic areas. Olivine and pyroxene show more ferroan compositions. Maskelynite is more alkali-rich.

The constituent minerals (pyroxene, maskelynite, and merrillite) are relatively enriched in LREE. The whole-rock (estimated) and the fusion crust of GRV 020090 are also enriched in LREE compared with typical "lherzolitic" shergottites, but quite similar to those of enriched shergottites. Combined with a high oxygen fugacity, it is evident that GRV 020090, similar to enriched basaltic shergottites, crystallized from a melt derived from an oxidized and enriched mantle reservoir. The calculated REE pattern of parent melt in equilibrium with the core of the low-Ca pyroxene oikocryst is parallel to that of the whole rock, indicating that all mineral phases in poikilitic and nonpoikilitic areas originated from a common parent melt and experienced closed-system fractional crystallization. The U-Pb age of baddeleyite in GRV 020090 is 192 ± 10 Ma. This age is in good agreement with the young internal isochron ages of other geochemically enriched shergottites. Multiple lines of evidence demonstrated that shergottites have young crystallization ages and that the 4.1 Ga Pb-Pb ages do not date the formation of shergottites.

GRV 020090 is another enriched "lherzolitic" shergottite after RBT 04261/2. They both exhibit a high content of maskelynite, more ferroan mineral compositions, LREE-enriched REE patterns, as well as almost identical crystallization ages. Comparison between GRV 020090 and RBT 04261/2 indicated that they are petrologically and geochemically closely related and probably launch paired. More extensive studies of these enriched "lherzolitic" shergottites could help clarify the petrogenetic relationships among shergottites.

Acknowledgments—Sample used in this study was provided by the Antarctic Meteorite Repository of Polar Research Institute of China (PRIC). The authors thank A. Irving, K. Misawa, and R. Korotev for their constructive reviews. This work was supported by the National Natural Science Foundation of China (Grant No. 41173076 and 10921063), by the Polar Strategic Research Foundation of China (20100207), and by the Minor Planet Foundation of China.

Editorial Handling—Dr. Randy Korotev

REFERENCES

Anand M., James S., Greenwood R. C., Johnson D., Franchi I. A., and Grady M. M. 2008. Mineralogy and geochemistry of shergottite RBT 04262 (abstract #2173). 39th Lunar and Planetary Science Conference. CD-ROM.

Barnes S. J. and Roeder P. L. 2001. The range of spinel compositions in terrestrial mafic and ultramafic rocks. *Journal of Petrology* 42:2279–2302.

Barrat J. A., Jambon A., Bohn M., Gillet P., Sautter V., Göpel C., Lesourd M., and Keller F. 2002. Petrology and chemistry of the picritic shergottite Northwest Africa 1068 (NWA 1068). *Geochimica et Cosmochimica Acta* 66:3505–3518.

Bindeman I. N., Davis A. M., and Drake M. J. 1998. Ion microprobe study of plagioclase-basalt partition experiments at natural concentration levels of trace elements. *Geochimica et Cosmochimica Acta* 62:1175–1193.

Borg L. E. and Drake M. J. 2005. A review of meteorite evidence for the timing of magmatism and of surface or near-surface liquid water on Mars. *Journal of Geophysical Research* 110:E12S03.

Borg L. E. and Draper D. S. 2003. A petrogenetic model for the origin and compositional variation of the Martian basaltic meteorites. *Meteoritics & Planetary Science* 38:1713–1731.

Borg L. E., Nyquist L. E., Wiesmann H., and Reese Y. 2002. Constraints on the petrogenesis of Martian meteorites from the Rb-Sr and Sm-Nd isotopic systematics of the lherzolitic shergottites ALHA77005 and LEW 88516. *Geochimica et Cosmochimica Acta* 66:2037–2053.

Borg L. E., Gaffney A. M., and DePaolo D. J. 2008. Preliminary age of Martian meteorite Northwest Africa 4468 and its relationship to the other incompatible-element-enriched shergottites (abstract #1851). 39th Lunar and Planetary Science Conference. CD-ROM.

Bouvier A., Blichert-Toft J., Vervoort J. D., and Albarède F. 2005. The age of SNC meteorites and the antiquity of the Martian surface. *Earth and Planetary Science Letters* 240:221–233.

Bouvier A., Blichert-Toft J., Vervoort J. D., Gillet P., and Albarède F. 2008. The case for old basaltic shergottites. *Earth and Planetary Science Letters* 266:105–124.

Bouvier A., Blichert-Toft J., and Albarède F. 2009. Martian meteorite chronology and the evolution of the interior of Mars. *Earth and Planetary Science Letters* 280:285–295.

Chen J. H. and Wasserburg G. J. 1986. Formation ages and evolution of Shergotty and its parent planet from U-Th-Pb systematics. *Geochimica et Cosmochimica Acta* 50:955–968.

Dreibus G., Jochum K. H., Palme H., Spettel B., Wlotzka F., and Wänke H. 1992. LEW 88516: A meteorite compositionally close to the "Martian mantle." *Meteoritics* 27:216–217.

Dreibus G., Spettel B., Haubold R., Jochum K. P., Palme H., Wolf D., and Zipfel J. 2000. Chemistry of a new shergottite: Sayh al Uhaymir 005 (abstract). *Meteoritics & Planetary Science* 35:A49.

Ebihara M., Kong P., and Shinotsuka K. 1997. Chemical composition of Y-793605, a Martian lherzolite. *Antarctic Meteorite Research* 10:83–94.

El Goresy A. 1965. Baddeleyite and its significance in impact glasses. *Journal of Geophysical Research* 70:3453–3456.

Fabriès J. 1979. Spinel-olivine geothermometry in peridotites from ultramafic complexes. *Contributions to Mineralogy and Petrology* 69:329–336.

Gaffney A. M., Borg L. E., and Connelly J. N. 2007. Uranium-lead isotope systematics of Mars inferred from the basaltic shergottite QUE 94201. *Geochimica et Cosmochimica Acta* 71:5016–5031.

Gillet P., Barrat J. A., Beck P., Marty B., Greenwood R. C., Franchi I. A., Bohn M., and Cotten J. 2005. Petrology, geochemistry, and cosmic-ray exposure age of lherzolitic shergottite Northwest Africa 1950. *Meteoritics & Planetary Science* 40:1175–1184.

Goodrich C. A. 2002. Olivine-phyric Martian basalts: A new type of shergottite. *Meteoritics & Planetary Science* 37:B31–B34.

Goodrich C. A., Herd C. D. K., and Taylor L. A. 2003. Spinels and oxygen fugacity in olivine-phyric and lherzolitic shergottites. *Meteoritics & Planetary Science* 38:1773–1792.

Harvey R. P., Wadhwa M., McSween H. Y., and Crozaz G. 1993. Petrography, mineral chemistry, and petrogenesis of Antarctic shergottite LEW 88516. *Geochimica et Cosmochimica Acta* 57:4769–4783.

Hays N. R., Drake M. J., and Gehrels G. G. 2011. U-Th-Pb analysis of baddeleyites in shergottite meteorites (abstract #1243). 42nd Lunar and Planetary Science Conference. CD-ROM.

Heaman L. M. 2009. The application of U-Pb geochronology to mafic, ultramafic and alkaline rocks: An evaluation of three mineral standards. *Chemical Geology* 261:43–52.

Herd C. D. K. 2003. The oxygen fugacity of olivine-phyric Martian basalts and the components within the mantle and crust of Mars. *Meteoritics & Planetary Science* 38:1793–1805.

Herd C. D. K. 2006. Insights into the redox history of the NWA 1068/1110 Martian basalt from mineral equilibria and vanadium oxybarometry. *American Mineralogist* 91:1616–1627.

Herd C. D. K., Papike J. J., and Brearley A. J. 2001. Oxygen fugacity of Martian basalts from electron microprobe oxygen and TEM-EELS analyses of Fe-Ti oxides. *American Mineralogist* 86:1015–1024.

Herd C. D. K., Borg L. E., Jones J. H., and Papike J. J. 2002. Oxygen fugacity and geochemical variations in the Martian basalts: Implications for Martian basalt petrogenesis and the oxidation state of the upper mantle of Mars. *Geochimica et Cosmochimica Acta* 66:2025–2036.

Herd C. D. K., Stern R. A., Walton E. L., Li J., and Bibby C. 2010. TEM and SEM-CL analysis of baddeleyite in NWA 3171: Geochronological implications for Martian meteorites (abstract #2280). 41st Lunar and Planetary Science Conference. CD-ROM.

Hsu W., Guan Y., Wang H., Leshin L. A., Wang R., Zhang W., Chen X., Zhang F., and Lin C. 2004. The lherzolitic shergottite Grove Mountains 99027: Rare earth element geochemistry. *Meteoritics & Planetary Science* 39:701–709.

Hui H., Peslier A. H., Lapen T. J., Shafer J. T., Brandon A. D., and Irving A. J. 2011. Petrogenesis of basaltic shergottite Northwest Africa 5298: Closed-system crystallization of an oxidized mafic melt. *Meteoritics & Planetary Science* 46:1313–1328.

Ikeda Y. 1997. Petrology and mineralogy of the Y-793605 Martian meteorite. *Antarctic Meteorite Research* 10:13–40.

Irving A. J., Kuehner S. M., Korotev R. L., and Hupé G. M. 2007. Petrology and bulk composition of primitive enriched olivine basaltic shergottite Northwest Africa 4468 (abstract #1526). 38th Lunar and Planetary Science Conference. CD-ROM.

Irving A. J., Kuehner S. M., Herd C. D. K., Gellissen M., Korotev R. L., Puchtel I., Walker R. J., Lapen T. J., and Rumble D. 2010. Petrologic, elemental and multi-isotopic characterization of permafic olivine-phyric shergottite Northwest Africa 5789: A primitive magma derived from depleted Martian mantle (abstract #1547). 41st Lunar and Planetary Science Conference. CD-ROM.

Lapen T. J., Brandon A. D., Beard B. L., Peslier A. H., Lee C.-T., and Dalton H. A. 2008. Lu-Hf age and isotope systematics of the olivine-phyric shergottite RBT 04262 and implications for the sources of enriched shergottites (abstract #2073). 39th Lunar and Planetary Science Conference. CD-ROM.

Le Maitre R. W., Dudek A., Keller J., Lameyre J., Le Bas M. J., Sabine P. A., Schmid R., Sørensen H., Streckeisen A., Woolley A. R., and Zanettin B. 1989. *A classification of igneous rocks and glossary of terms: Recommendations of the International Union of Geological Sciences Subcommission on the Systematics of Igneous Rocks*. Oxford, UK: Blackwell Scientific Publications. 193 p.

Li Q., Li X., Liu Y., Tang G., Yang J., and Zhu W. 2010. Precise U-Pb and Pb-Pb dating of Phanerozoic baddeleyite by SIMS with oxygen flooding technique. *Journal of Analytical Atomic Spectroscopy* 25:1107–1113.

Li Q., Li X., Wu F., Yin Q., Ye H., Liu Y., Tang G., and Zhang C. 2012. In-situ SIMS U-Pb dating of phanerozoic apatite with low U and high common Pb. *Gondwana Research* 21:745–756.

Lin Y., Guan Y., Wang D., Kimura M., and Leshin L. A. 2005. Petrogenesis of the new lherzolitic shergottite Grove Mountains 99027: Constraints of petrography, mineral chemistry, and rare earth elements. *Meteoritics & Planetary Science* 40:1599–1619.

Lin Y., Liu T., Shen W., Xu L., and Miao B. 2008a. Grove Mountains (GRV) 020090: A highly fractionated lherzolitic shergottite (abstract #5076). 71st Annual Meteoritical Society Meeting. CD-ROM.

Lin Y., Qi L., Wang G., and Xu L. 2008b. Bulk chemical composition of lherzolitic shergottite Grove Mountains (GRV) 99027—Constraints on the mantle of Mars. *Meteoritics & Planetary Science* 43:1179–1187.

Lindsley D. H. 1983. Pyroxene thermometry. *American Mineralogist* 68:477–493.

Liu Y., Hu Z., Gao S., Günther D., Xu J., Gao C., and Chen H. 2008. In situ analysis of major and trace elements of anhydrous minerals by LA-ICP-MS without applying an internal standard. *Chemical Geology* 257:34–43.

Liu Y., Li X., Li Q., Tang G., and Yin Q. 2011. Precise U-Pb zircon dating at a scale of < 5 micron by the CAMECA 1280 SIMS using a Gaussian illumination probe. *Journal of Analytical Atomic Spectrometry* 26:845–851.

Lodders K. 1998. A survey of shergottites, nakhlite, and chassigny meteorites whole-rock compositions (abstract). *Meteoritics & Planetary Science* 33:A183–A190.

Ludwig K. R. 2001. *User's manual for Isoplot/Ex rev. 2.49. A geochronological toolkit for Microsoft Excel*. Berkeley, California: Berkeley Geochronology Centre Special Publication 1a. 56 p.

Lundberg L. L., Crozaz G., Mckay G. A., and Zinner E. 1988. Rare earth element carriers in the Shergotty meteorite and implications for its chronology. *Geochimica et Cosmochimica Acta* 52:2147–2163.

Lundberg L. L., Crozaz G., and McSween H. Y. 1990. Rare earth elements in minerals of the ALHA77005 shergottite and implications for its parent magma and crystallization history. *Geochimica et Cosmochimica Acta* 54:2535–2547.

Ma M. S., Laul J. C., and Schmitt R. A. 1981. Complementary rare earth element patterns in unique achondrites, such as ALHA77005 and shergottites, and in the Earth. Proceedings, 12th Lunar and Planetary Science Conference. pp. 1349–1358.

Marks N. E., Borg L. E., Gaffney A. M., and DePaolo D. 2010. The relationship of Northwest Africa 4468 to the other incompatible-element-enriched shergottites inferred from its Rb-Sr and Sm-Nd isotopic systematics (abstract #2064). 41st Lunar and Planetary Science Conference. CD-ROM.

McCanta M. C., Rutherford M. J., and Jones J. H. 2004. An experimental study of rare earth element partitioning between a shergottite melt and pigeonite: Implications for the oxygen fugacity of the Martian interior. *Geochimica et Cosmochimica Acta* 68:1943–1952.

Miao B., Ouyang Z., Wang D., Ju Y., Wang G., and Lin Y. 2004. A new Martian meteorite from Antarctica: Grove Mountains (GRV) 020090. *Acta Geologica Sinica* 78:1034–1041.

Mikouchi T. 2005. Northwest Africa 1950: Mineralogy and comparison with Antarctic lherzolitic shergottites. *Meteoritics & Planetary Science* 40:1621–1634.

Mikouchi T. 2009. Petrological and mineralogical diversities within the lherzolitic shergottites require a new group name (abstract #2272)? 40th Lunar and Planetary Science Conference. CD-ROM.

Mikouchi T. and Miyamoto M. 2000. Lherzolitic Martian meteorites Allan Hills 77005, Lewis Cliff 88516 and Yamato-793605: Major and minor element zoning in pyroxene and plagioclase glass. *Antarctic Meteorite Research* 13:256–269.

Mikouchi T., Kurihara T., and Miyamoto M. 2008. Petrology and mineralogy of RBT 04262: Implications for stratigraphy of the lherzolitic shergottite igneous block (abstract #2403). 39th Lunar and Planetary Science Conference. CD-ROM.

Misawa K., and Yamaguchi A. 2007. U-Pb ages of NWA 856 baddeleyite (abstract #5228). 70th Annual Meteoritical Society Meeting. CD-ROM.

Neukum G., Basilevsky A. T., Kneissl T., Chapman M. G., van Gasselt S., Michael G., Jaumann R., Hoffmann H., and Lanz J. K. 2010. The geologic evolution of Mars: Episodicity of resurfacing events and ages from cratering analysis of image data and correlation with radiometric ages of Martian meteorites. *Earth and Planetary Science Letters* 294:204–222.

Niihara T. 2011. Uranium-lead age of baddeleyite in shergottite Roberts Massif 04261: Implications for magmatic activity on Mars. *Journal of Geophysical Research* 116:E12008.

Niihara T., Kaiden H., Misawa K., and Sekine T. 2009a. U-Pb isotopic systematics of experimentally shocked baddeleyite (abstract #1562). 40th Lunar and Planetary Science Conference. CD-ROM.

Niihara T., Kaiden H., Misawa K., and Sekine T. 2009b. Shock metamorphism on baddeleyite: Implication for U-Pb isotopic systematic of shergottites (abstract #5274). 72nd Annual Meteoritical Society Meeting. CD-ROM.

Nyquist L. E., Bogard D. D., Shih C.-Y., Greshake A., Stöffler D., and Eugster O. 2001. Ages and geologic histories of Martian meteorites. *Space Science Reviews* 96:105–164.

Nyquist L. E., Bogard D. D., Shih C.-Y., Park J., Reese Y. D., and Irving A. J. 2009. Concordant Rb-Sr, Sm-Nd, and Ar-Ar ages for Northwest Africa 1460: A 346 Ma old basaltic shergottite related to "lherzolitic" shergottites. *Geochimica et Cosmochimica Acta* 73:4288–4309.

Ohtaka O., Fukui H., Kunisada T., Fujisawa T., Funakoshi K., Utsumi W., Irifune T., Kuroda K., and Kikegawa T. 2001. Phase relations and equations of state of ZrO_2 under high temperature and high pressure. *Physical Review B* 63:174108-1–174108-8.

Peslier A. H., Hnatyshin D., Herd C. D. K., Walton E. L., Brandon A. D., Lapen T. J., and Shafer J. T. 2010. Crystallization, melt inclusion, and redox history of a Martian meteorite: Olivine-phyric shergottite Larkman Nunatak 06319. *Geochimica et Cosmochimica Acta* 74:4543–4576.

Rubin A. E., Warren P. H., Greenwood J. P., Verish R. S., Leshin L. A., Hervig R. L., Clayton R. N., and Mayeda T. K. 2000. Los Angeles: The most differentiated basaltic Martian meteorite. *Geology* 28:1011–1014.

Sack R. O. and Ghiorso M. S. 1991. Chromian spinels as petrogenetic indicators: Thermodynamics and petrologic applications. *American Mineralogist* 76:827–847.

Satterwhite C. and Righter K. 2007. New meteorites—Shergottites and ungrouped chondrites. *Antarctic Meteorite Newsletter* 30:1–20.

Shafer J. T., Brandon A. D., Lapen T. J., Righter M., Peslier A. H., and Beard B. L. 2010. Trace element systematics and Sm-Nd and Lu-Hf ages of Larkman Nunatak 06319: Closed-system fractional crystallization of an enriched shergottite magma. *Geochimica et Cosmochimica Acta* 74:7307–7328.

Shih C. Y., Nyquist L. E., Bogard D. D., Mckay G. A., Wooden J. L., Bansal B. M., and Wiessmann H. 1982. Chronology and petrogenesis of young achondrites, Shergotty, Zagami, and ALHA77005: Late magmatism on a geologically active planet. *Geochimica et Cosmochimica Acta* 46:2323–2344.

Stacey J. S. and Kramers J. D. 1975. Approximation of terrestrial lead isotope evolution by a two-stage model. *Earth and Planetary Science Letters* 26:207–221.

Stolper E. and McSween H. Y. 1979. Petrology and origin of the shergottite meteorites. *Geochimica et Cosmochimica Acta* 43:1475–1477.

Symes S. J. K., Borg L. E., Shearer C. K., and Irving A. J. 2008. The age of the Martian meteorite Northwest Africa 1195 and the differentiation history of the shergottites. *Geochimica et Cosmochimica Acta* 72:1696–1710.

Tera F. and Wasserburg G. J. 1972. U-Th-Pb systematics in three Apollo 14 basalts and the problem of initial Pb in lunar rocks. *Earth and Planetary Science Letters* 14:281–304.

Treiman A. H. 2003. Chemical compositions of Martian basalts (shergottites): Some inferences on basalt formation, mantle metasomatism, and differentiation in Mars. *Meteoritics & Planetary Science* 38:1849–1864.

Usui T., Sanborn M., Wadhwa M., and McSween H. Y. 2010. Petrology and trace element geochemistry of Robert Massif 04261 and 04262 meteorites, the first examples of geochemically enriched lherzolitic shergottites. *Geochimica et Cosmochimica Acta* 74:7283–7306.

Van de Moortèle B., Reynard B., Rochette P., Jackson M., Beck P., Gillet P., McMillan P. F., and McCammon C. A. 2007. Shock-induced metallic iron nanoparticles in olivine-rich Martian meteorites. *Earth and Planetary Science Letters* 262:37–49.

Wadhwa M. 2001. Redox state of Mars' upper mantle and crust from Eu anomalies in shergottite. *Science* 291:1527–1530.

Wadhwa M., McSween H. Y., and Crozaz G. 1994. Petrogenesis of shergottite meteorites inferred from minor and trace element microdistributions. *Geochimica et Cosmochimica Acta* 58:4213–4229.

Wadhwa M., Mckay G. A., and Crozaz G. 1999. Trace element distributions in Yamato-793605, a chip off the "Martian lherzolite" block. *Antarctic Meteorite Research* 12:168–182.

Wittmann A., Kenkmann T., Schmitt R. T., and Stöffler D. 2006. Shock-metamorphosed zircon in terrestrial impact craters. *Meteoritics & Planetary Science* 41:433–454.

Wood B. J., Bryndzia L. T., and Johnson K. E. 1990. Mantle oxidation state and its relationship to tectonic environment and fluid speciation. *Science* 248:337–345.

Zipfel J., Scherer P., Spettel B., Dreibus G., and Schultz L. 2000. Petrology and chemistry of the new shergottite Dar al Gani 476. *Meteoritics & Planetary Science* 35:95–106.